

Gait Simulation Pilot Project: Changes in the Shock Dissipation Mechanism of the Lower Extremity Due to Varying Gravity Loads

S. McGuan
Mechanical Dynamics Inc.

INTRODUCTION

The purpose of this project is to utilize a human musculoskeletal model developed previously for foot disease gait correction [1] to determine the kinematic, kinetic and ground reaction force dissipation signatures at various gravity constants. The changes in the signatures for the various gravity loads will provide an indication of how the energy dissipation mechanism in the foot (pronation: coupled eversion/abduction/dorsiflexion) adapts to the changing effective body weight.

METHODS

A computer model representing a 115 lb. barefoot male consisted of a single mass element representing the body, and two lower extremities. Figure 1 displays the detailed right lower extremity.

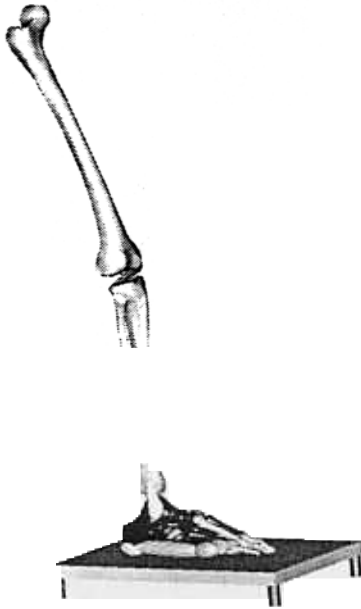


Figure 1. Lower Extremity Model at Full Forefoot Load

Segments

The musculoskeletal lower extremity model consisted of 12 segments (bones) and 15 monocentric single-degree-of-freedom hinge joints. The plantar soft tissue was modeled as a contact force using separate ellipsoidal elements. The femur and tibia-fibula were modeled as segments joined by 2 dof knee joint permitting both flexure and tibial rotation. For the foot, the talus, calcaneus and 5 metatarsals were each modeled as rigid bodies. A lumping scheme similar in principal to Scott [2] is employed where the navicular, the cuboid and the three cuneiform bones are combined into one rigid part.

Joints

The ankle (talocrural) joint provides rotation between the talus and the tibia, and the subtalar (talocalcaneal) joint provides

rotation between the talus and the calcaneus. Recent studies found that the angular motion of the subtalar joint during walking can be represented adequately by a single dof, monocentric joint [3]. Based on this study and others [4], all joints in the model were modeled as simple hinge joints. These hinge joints have a specific orientation and range of motion, and are dependent on the local physiology. The average axis of motion for the ankle joint lies approximately 8° to the transverse plane and $20^\circ - 30^\circ$ to the frontal plane [5]. Figure 2 displays the ankle joint axis orientation.

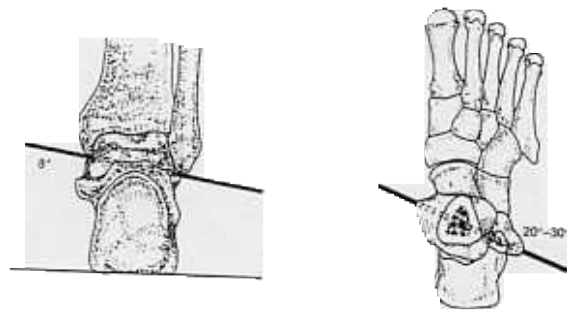


Figure 2. Average Axis of Motion for the Ankle Joint.

Motion in the average subtalar joint occurs about an axis that lies 42° to the transverse plane and 23° to the sagittal plane. The position of this axis allows for tri-planar motion with almost equal amounts of frontal (eversion/inversion) and transverse planar motion (adduction/abduction). This action can be compared to the motion of a mitered hinge [8]. Figure 3 displays the subtalar joint axis orientation.

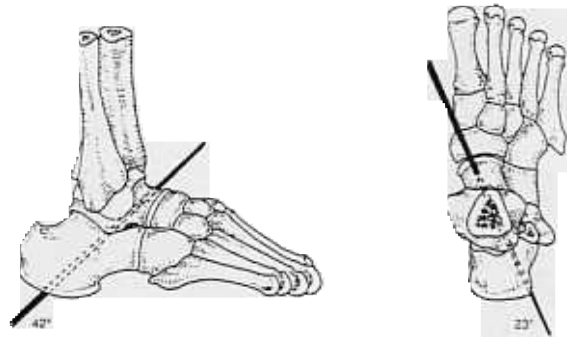


Figure 3. Average Axis of Motion for the Subtalar Joint.

The midtarsal joint consists of the combined articulations between the talonavicular and calcaneocuboid joints. These joints function as a unit to allow for tri-planar motion that occurs about two distinct axes: the oblique midtarsal joint axis (OMJA) and the longitudinal midtarsal joint axis (LMJA) [9]. The default orientations [10] for the OMJA is 52° to the transverse plane and 57° to the sagittal plane, where as the LMJA lies 15° to

transverse plane and 9° to the sagittal plane. Figure 4 displays the default orientations for the LMJA and OMJA joints.

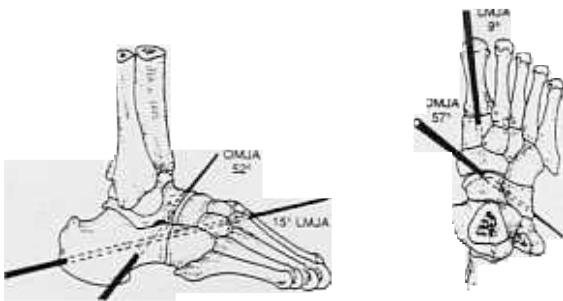


Figure 4. Average Axis of Motion for the OMJA and LMJA.

For this study, the reported average joint alignments are used, however, in practice the clinician may reposition this axis based on palpitation measurements through and evaluation procedure [6,7]. The limits of angulation for each joint also vary from subject to subject and for this study, the reported average is used. These limits, however, are easily determined from patient evaluation and may be entered into the system by the clinician.

Muscle Forces

Muscle forces acting across each joint in the model (knee flexure, tibial flexure, ankle motion, subtalar motion OMJA and LMJA motion) control the trajectory of each part and subsequently the functional kinematics for the lower extremity computer model during the gait simulation. To implement muscle forces in the model, special subroutines were developed to describe the composite torques representing an estimation of the cumulative effect of the musculature acting in the local region. Due to the fact that there are many contributing muscle groups, each with distinct mechanical and physiological properties, activation rates and insertion points which are patient specific, it is only practical for this present study to model muscle action using composite torques [11]. Also, by simulating the heel-strike through the full forefoot loading of the gait cycle, the foot is in the mobile adapter stage where there are minimal correction mechanisms [12,13] and it is functionally acceptable to model the supporting musculature as non-linear, responsive, spring-damper torque functions. The torque functions at each joint employ a curve form displayed in figure 5, which couples operational resistance activity with the individual physiological range-of-motion joint limits.

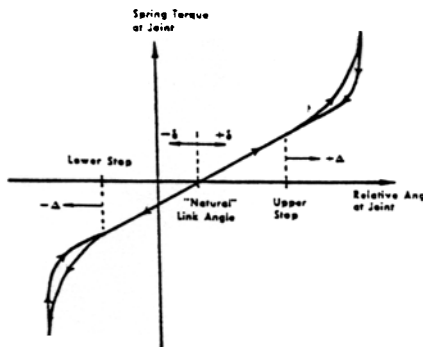


Figure 5. Joint Resistance Torque Curve Form.

The parameters in these torque functions are maximum and minimum angles (physiological joint limit), neutral angle, stiffness, stiffness exponent (for non-linear resistance) and damping values. The range-of-motion values (maximum and minimum angles) and the neutral angles are input from patient measurements. This stiffness and damping values are developed from a calibration process detailed in the next section. For each parameter, the model in this study contains the default values which were derived from the calibration process, for a patient with a normal foot condition.

Contact Forces

The contact forces generated between the heel, hallux and 5 metatarsal heads are modeled using contact forces based on ellipsoidal contact elements. The contact algorithm uses these elements to calculate the volume of penetration of the ellipsoid into the contact plane generating normal and frictional forces. The normal force is calculated using compliance data representing the contact between the fat pad of the plantar surface of the foot and the floor provided in Valient [14]. Figure 6 displays the foot model with the contact elements.

BOTTOM VIEW



Figure 6. Ellipsoidal Contact Elements for Skin/Ground Contact.

Gait Simulation Calibration

The human model was calibrated to match the kinematic data and muscle activation cycle data for a portion of the gait cycle consisting of heel-strike through full forefoot load, as reported by Michaud [6]. These data were used as a guide when developing the stiffness and damping parameters for the muscle torque functions. To do the calibration, an optimization scheme [17] was developed to alter parameters based on the output from the model (knee flexure, tibial rotation, ankle motion, subtalar motion, OMJA motion and LMJA motion) as compared against a target [6]. The target data is listed in figures 7-12.

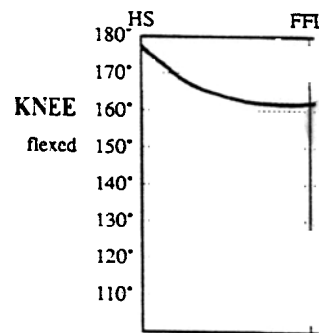


Figure 7. Knee Flexure Motion Target.

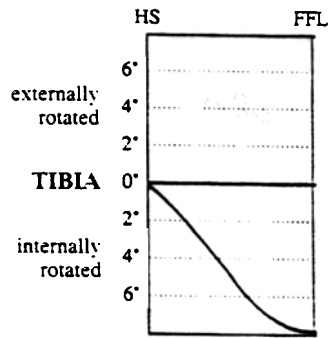


Figure 8. Tibial Rotation Motion Target.

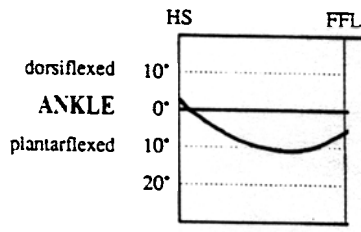


Figure 9. Ankle Motion Target.

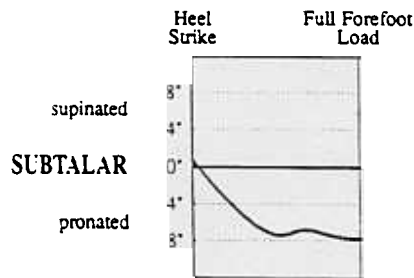


Figure 10. Subtalar Flexure Motion Target.

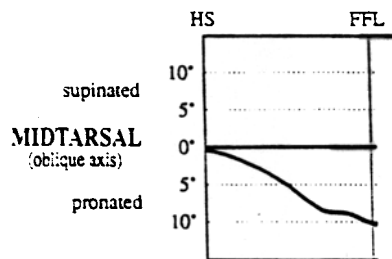


Figure 11. OMJA Flexure Motion Target.

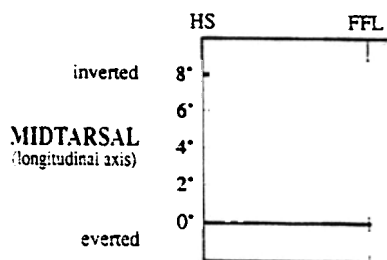


Figure 12. LMJA Flexure Motion Target.

These data are indicators of lower extremity functional kinematics during the gait cycle. These data indicate that at the moment that heel-strike occurs, the knee is fully extended; the ankle is slightly dorsiflexed; the subtalar joint is slightly supinated; and the midtarsal joint is fully pronated about its oblique axis and supinated (inverted about its longitudinal axis) (see fig. 13). As the foot proceeds through its contact period, a combination of ground-reactive force (which are initially applied to the posterolateral heel) and inertial forces (the pelvis and lower extremity continue their internal rotation, which began during early swing phase) causes the ankle to plantar flex and the subtalar joint to pronate. Plantarflexion of the ankle is resisted by eccentric contraction of the anterior compartment musculature [15]. The ankle continues to plantarflex throughout the first 70% of the contact period, reaching a maximally plantarflexed position of 10°. At that time, the ground-reactive force beneath the forefoot cause the ankle to dorsiflex slightly (i.e., the ankle is still plantarflexed by 5° by the end of the contact period). The contact period ends with full forefoot loading. Throughout the entire contact period, the subtalar joint is pronating from the slightly supinated position presented at heel-strike. An extremely important clinical consideration is that subtalar joint pronation is both directly and indirectly responsible for shock absorption. Root [16] stresses the significance of this by noting that any condition preventing the normal range of subtalar joint pronation will result in pathological amounts of stress being transmitted up the leg, into the pelvis and lumbar spine. Figure 13-15 display the animation sequences for the gait simulation of a healthy profile.

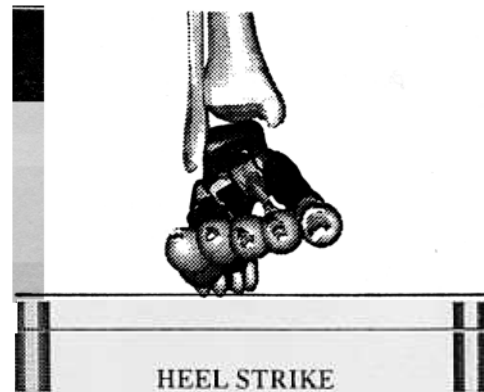


Figure 13 Heel-Strike Phase of Gait Cycle (sim time = 0s)

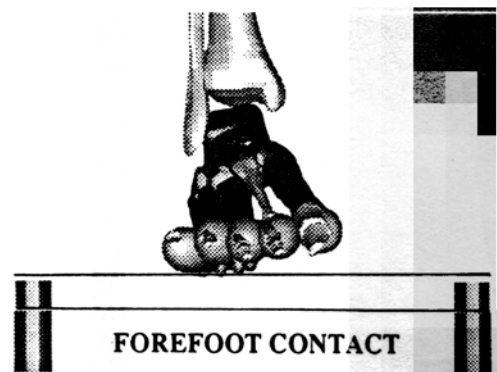


Figure 14. Forefoot Touch Phase of Gait Cycle (sim time = 25s)

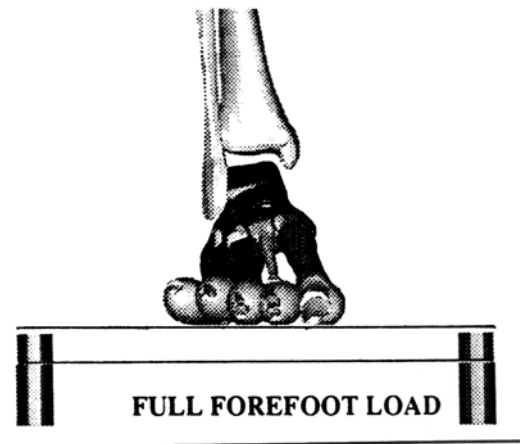


Figure 15. Full Forefoot Loading (sim time = .5s)

Model Data

The behavior of the model to these gait conditions can be detailed in three types of signatures: Kinematic, Kinetic and Ground Reaction Force (GRX) Dissipation. The kinematic signature data includes ankle, subtalar, longitudinal metatarsal joint axis, oblique metatarsal joint axis, tibial and knee flexion rotations. The kinetic signature data includes torques reported at the ankle joint, subtalar joint, longitudinal metatarsal joint axis, oblique metatarsal joint axis, tibial axial (at knee), and knee flexure. The GRX dissipation signature data includes joint impact forces at the force plate, ankle joint, knee joint and the hip joint.

RESULTS

Walking gait simulations for a barefoot patient weighing 115.39 lbs. were performed. The portion of the gait cycle recorded was heel-strike through full forefoot load. Data was collected for the right extremity. During the simulation the left extremity was assumed to be in contact with the floor to provide support. Plots 1-16 detail the kinematic, kinetic and GRX dissipation signatures for the gait cycle under gravity loads of 1.0, .8, .6, .4 and .2. Simulations performed for the model under 0 gravity resulted in unrealistic motion and subsequently the results were discarded. Simulations were performed for a full second, however, full forefoot load occurs at approximately .5 seconds for each case.

Kinematic Signature

Plots 1-6 display the kinematic signature for model under the gravity conditions of GC = 1, .8, .6, .4, and .2. For the various gravity loads, the kinematics of the lower extremity change noticeably, especially in knee flexion where hardly any flexion occurs at a GC of .2. Due to the non-linear torque relationships and geometries, the changes in the kinematic signature for each gravity load case is not linear as can be observed in Plot 1. Generally the trends of the plot demonstrate the decreased reliance on the shock dissipation mechanism of the lower extremity under decreasing gravity conditions. This is evidenced in all three signatures.

Kinetic Signature

Plots 7-12 display the kinetic signature for model under the gravity conditions of GC = 1, .8, .6, .4, and .2. As with the kinematic signature, the kinetic signature also indicates the

decreased reliance on the shock absorption mechanism of the lower extremity, most notably in the knee flexion with a maximum torque of ~ 26000 N - mm for a GC = 1 to a torque of ~ 100 N - mm for a GC of .2.

GRX Dissipation Signature

Plots 13-16 display the GRX dissipation signature for model under the gravity conditions of GC = 1, .8, .6, .4, and .2. The plots indicate how the shock dissipation mechanism of the lower extremity absorbs the GRX as evidenced by the decreased joint force from the GRX through the ankle, knee and hip. The shape of the GRX curves exhibit the classic double peak curve shape common to bare foot gait [18]. The larger sharper peak (passive peak) is due to the sharp impact of the barfoot heel on the force plate surface. The second peak (active) is due to the mid and forefoot impact on the force plate surface.

Effective joint shock may be estimated from the GRX dissipation signature curves by adding both the active and passive peaks. GRX shock transmission at each joint may be calculated by determining the percentage of the GRX reduction at that particular joint site. Table 1 displays the values of GRX shock absorption.

Table 1: GRX Shock Absorption

	GC = 1	GC=.8	GC=.6	GC=.4	GC=.2
Floor Shock	100%	100%	100%	100%	100%
Ankle Shock	93%	99%	94%	96%	93%
Knee Shock	82%	84%	83%	85%	85%
Hip Shock	63%	66%	65%	66%	66%

The table provides data on how the GRX shock is transmitted through the extremity to the hip. The decreasing percentages indicate the performance of local shock dissipation mechanisms for the extremity. The general trend, comparing 63% shock transmission at the hip for a GC of 1 to 66% shock transmission at the hip for a GC of .2, indicates that at lesser gravity the shock absorption mechanism absorbs less relative shock.

CONCLUSION

Obviously this current study is limited. The intention of the scope of this project is to serve as pilot project to generate data relevant to reported experimental results: To generate kinematic, kinetic and shock dissipation data to demonstrate the changing shock absorption mechanisms in the human lower extremity due to changing gravity loads. This study also serves the support the usage of computerized, mechanical modeling of human function as a viable scientific method. The intrinsic benefits of using virtual human models for functional analysis are numerous including: rapid data acquisition, fast model/environment changes, more detailed data than experiment (internal variables), greater visualization, greater inter-experiment consistency, etc.

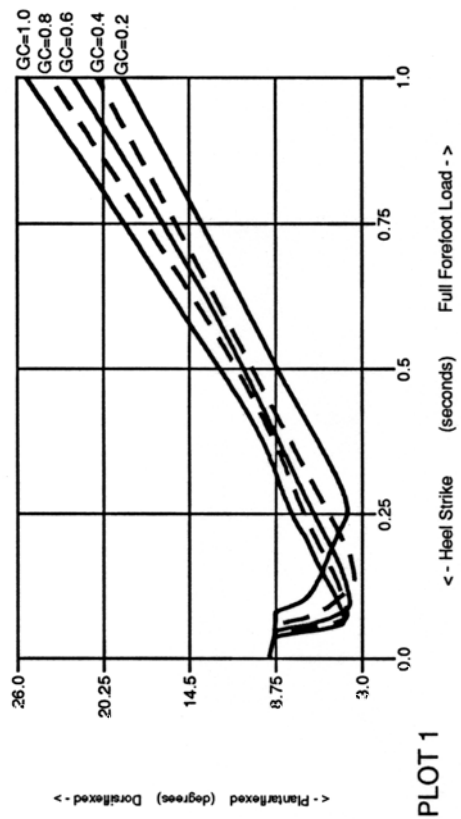
FUTURE WORK

The techniques and algorithms developed for this particular study may be expanded in two major areas to include much more detail to address many more scientific issues. The areas of future model development include muscle force and CNS motor control. Past MDI projects have included Hill muscle formulations as actuation forces in human models. There is continued debate on the relevancy of the current Hill muscle model, and these human models can be used to test and evaluate new muscle force derivations. In the area of CNS motor control, simple PID controllers and optimization schemes have been employed in the past to allow for the human model to walk using Hill muscle formulations. Future work would include the usage of neural networks (neural oscillators) to control the muscle forces in the model. Utilizing the newly introduced, real-time link between ADAMS[®] and MatrixX[®] or ADAMS and Matlab[®], the development and utilization of this type of human control is now possible.

REFERENCES

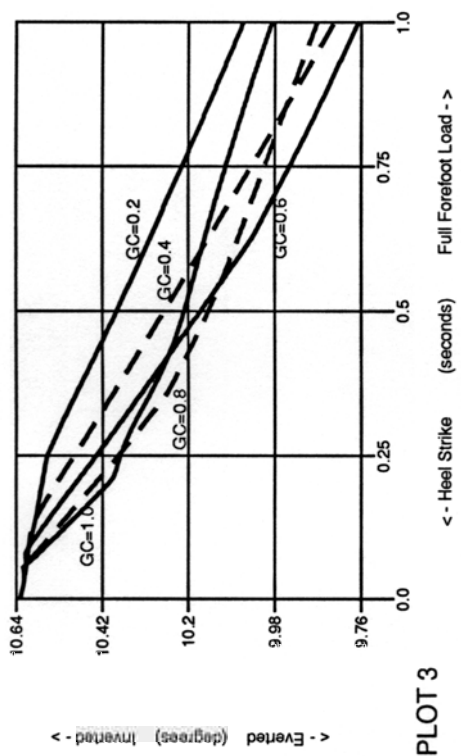
- [1] McGuan, S.P., (1996) "Personalized Musculoskeletal Human Models for use in Dynamic Gait Simulation for Clinical and Sports Applications", *Portuguese Journal of Human Performance Studies*.
- [2] Scott, S. et al. (1993) "Biomechanical Model of the Human Foot: Kinematics and Kinetics During the Stance Phase of Walking", *Journal of Biomechanics*.
- [3] Scott, S. et al. (1991) "Talocrural and Talocalcaneal Joint Kinematics and Kinetics During the Stance Phase of Walking", *Journal of Biomechanics*.
- [4] Robertson, D.G., (1980) "Mechanical Energy Generation, Absorption and Transfer Amongst Segments During Walking", *Journal of Biomechanics*.
- [5] Harris, G.F., (1991) "Analysis of Ankle and Subtalar Motion During Human Locomotion" Inman's Joints of the Ankle, Williams and Wilkins.
- [6] Michaud, T., (1993) Foot Orthoses and Other Forms of Conservative Foot Care, Williams and Wilkins.
- [7] Donatelli, R., (1990) The Biomechanics of the Foot and Ankle, F.A. Davis.
- [8] Inman, V.T., et al. (1978) "Biomechanics of the Foot and Ankle", DuVries' Surgery of the Foot CV Mosby
- [9] Hicks, J.H., (1954) "The Mechanics of the Foot", *Journal of Anatomy*.
- [10] Manter, J.T., (1941) "Movements of the Subtalar and Transverse Tarsal Joints", *Anat. Rec.*
- [11] Winters, J.M., et al., (1991) Multiple Muscle Systems, Springer-Verlag.
- [12] Alexander, R.M., et al. (1975) "The Dimensions of the Knee and Ankle Muscles and the Forces They Exert", *Journal of Human Movement Studies*.
- [13] D'Ambrasia, R.D., et al. (1989) *Running Injuries*, Slack Inc.
- [14] Valiant, G.A., (1984) "A Determination of the Mechanical Characteristics of the Human Heel Pad in Vivo", Ph.D. Thesis, Pennsylvania State University.
- [15] Basmajian, J.V., et al. (1985) Muscles Alive: Their Functions Revealed by Electromyography, Williams and Wilkins.
- [16] Root M.C., et al. (1977) "Normal and Abnormal Function of the Foot", *Los Angeles: Clinical Biomechanics*.
- [17] Pike R. (1986) Optimization for Engineering Systems, Van Nostrand Reinhold Publishers.
- [18] Bobbert M. (1989) "Shock Attenuation in Locomotion" *Journal of Biomechanics*

KINEMATIC SIGNATURE
ANKLE ROTATION Patient=lst



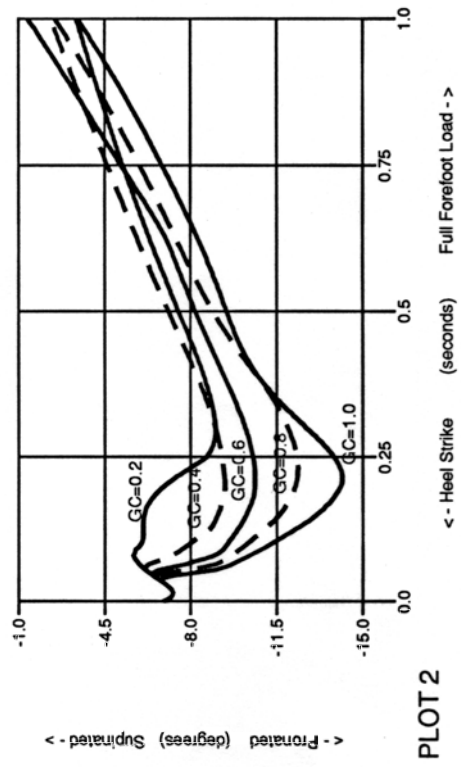
PLOT 1

KINEMATIC SIGNATURE
LMJA ROTATION Patient=lst



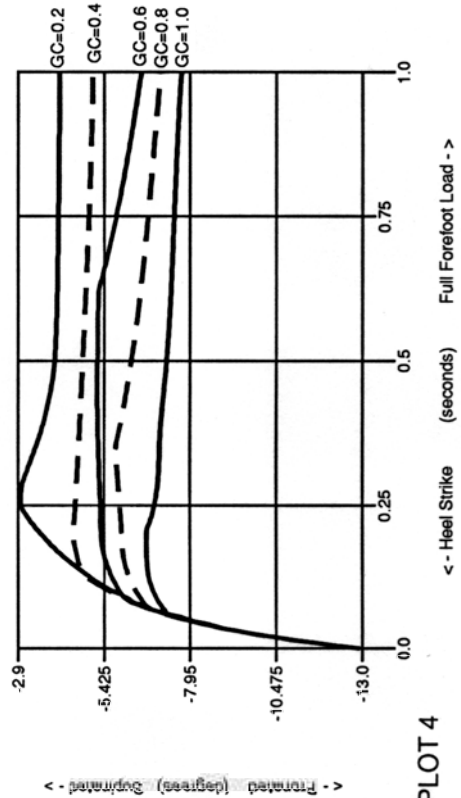
PLOT 3

KINEMATIC SIGNATURE
SUBTALAR ROTATION Patient=lst



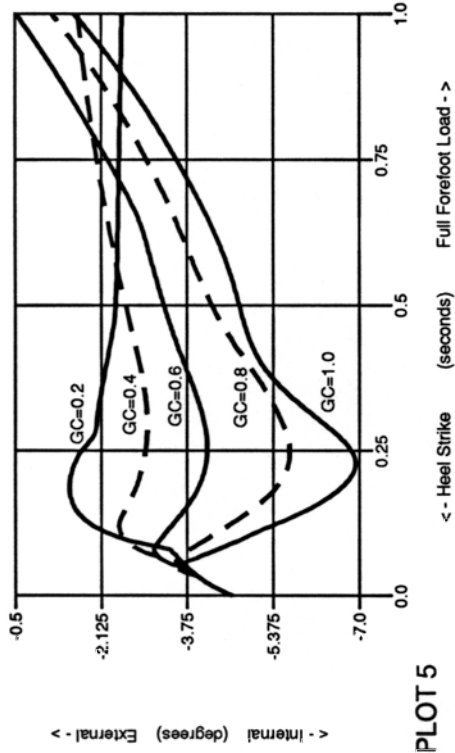
PLOT 2

KINEMATIC SIGNATURE
OMJA ROTATION Patient=lst



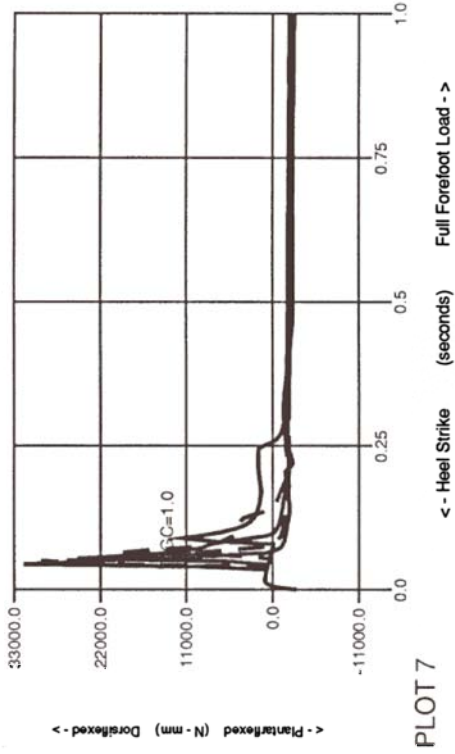
PLOT 4

KINEMATIC SIGNATURE
TIBIAL ROTATION Patient=1st



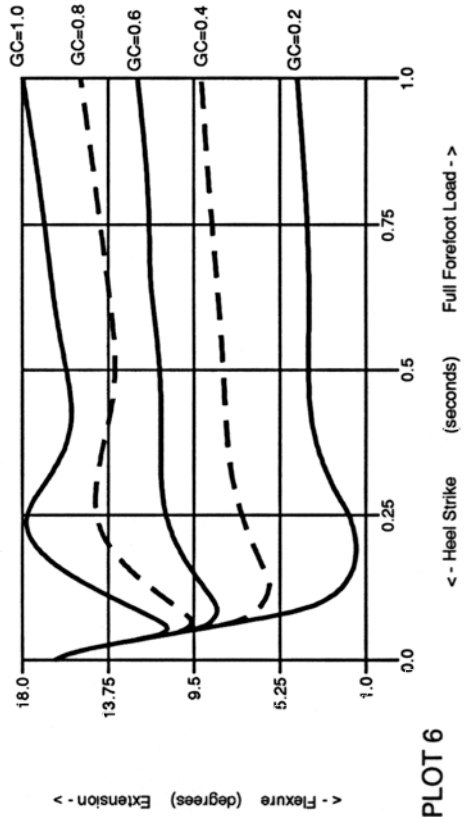
PLOT 5

KINEMATIC SIGNATURE
ANKLE TORQUE Patient=1st



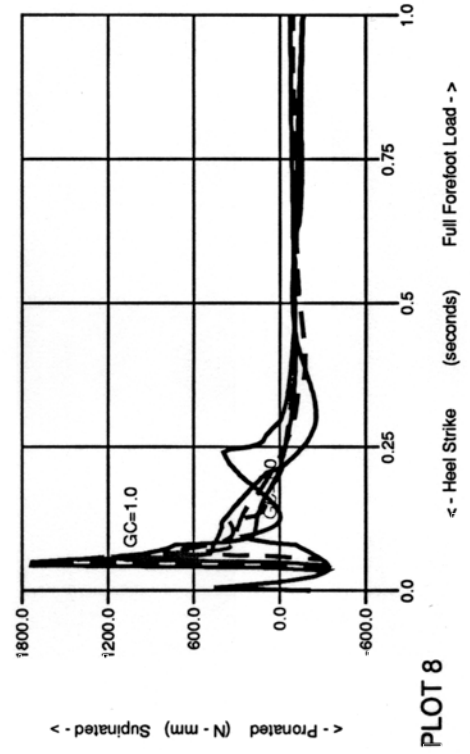
PLOT 7

KINEMATIC SIGNATURE
KNEE FLEXION Patient=1st



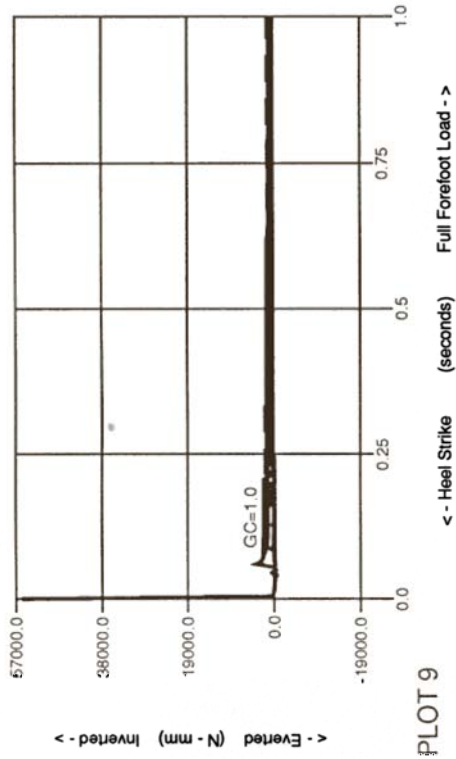
PLOT 6

KINEMATIC SIGNATURE
SUBTALAR TORQUE Patient=1st



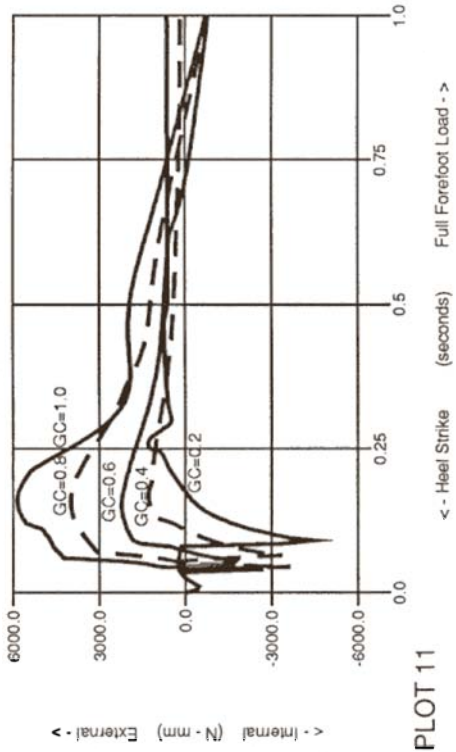
PLOT 8

KINETIC SIGNATURE
LMAJ TORQUE Patient=1st



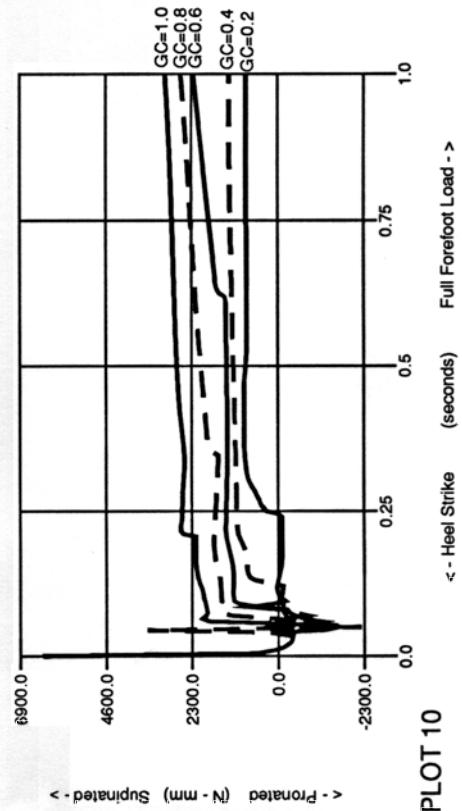
PLOT 9

KINETIC SIGNATURE
TIBIAL AXIAL TORQUE Patient=1st



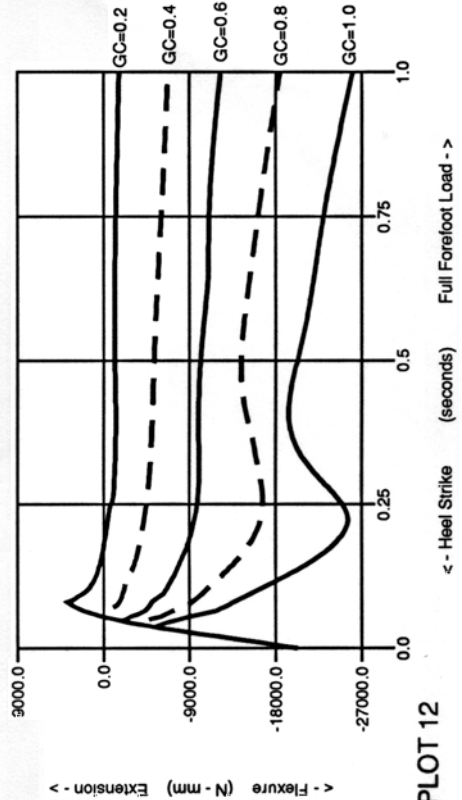
PLOT 11

KINETIC SIGNATURE
OMJA TORQUE Patient=1st



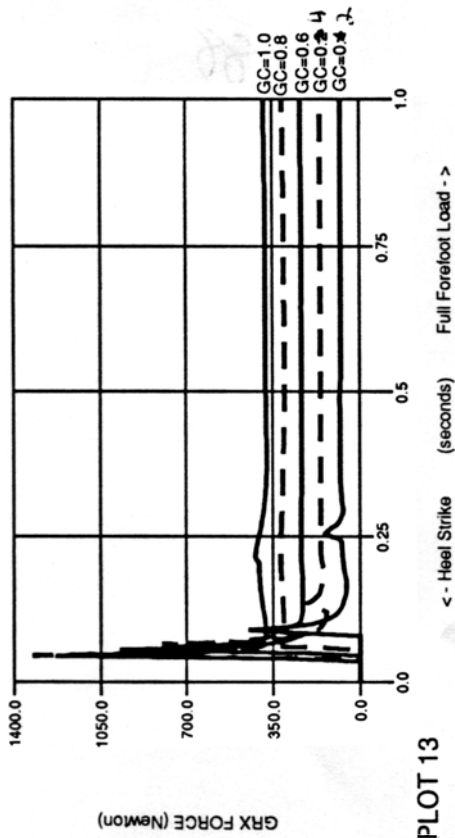
PLOT 10

KINETIC SIGNATURE
KNEE FLEXURE TORQUE Patient=1st



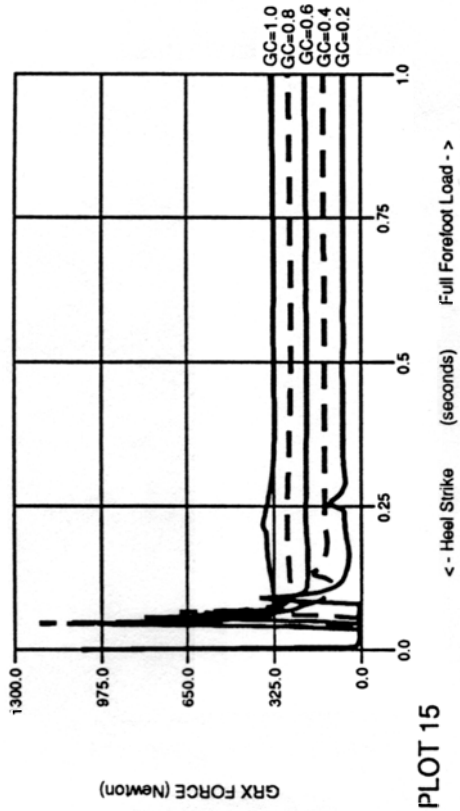
PLOT 12

GRX DISSIPATION SIGNATURE
GROUND REACTION FORCE Patient-1st



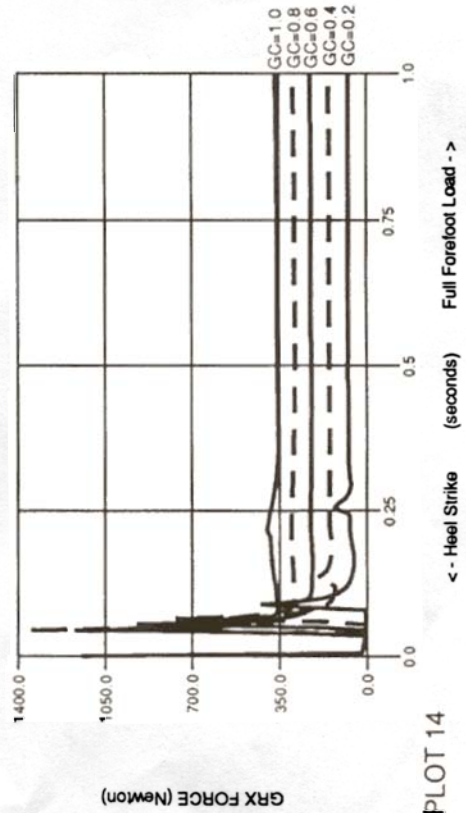
PLOT 13

GRX DISSIPATION SIGNATURE
GRX AT KNEE JOINT Patient-1st



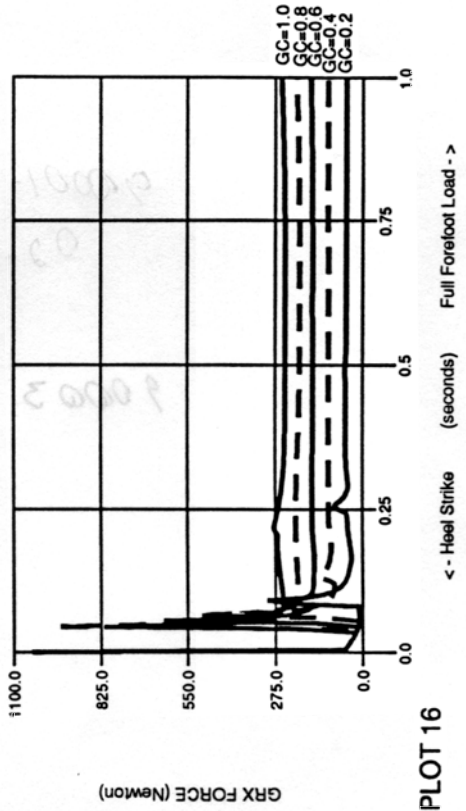
PLOT 15

GRX DISSIPATION SIGNATURE
GRX AT ANKLE JOINT Patient-1st



PLOT 14

GRX DISSIPATION SIGNATURE
GRX AT HIP JOINT Patient-1st



PLOT 16